Sādhanā Vol. 31, Part 5, October 2006, pp. 583–595. © Printed in India

Analytical model for erosion behaviour of impacted fly-ash particles on coal-fired boiler components

S K DAS, K M GODIWALLA, S P MEHROTRA, K K M SASTRY and P K DEY

National Metallurgical Laboratory, Jamshedpur 831 007, India
e-mail: skd@nmlindia.org

MS received 15 July 2005; revised 14 August 2006

Abstract. Fly ash particles entrained in the flue gas from boiler furnaces in coal-fired power stations can cause serious erosive wear on steel surfaces along the flow path. Such erosion can significantly reduce the operational life of the boiler components. A mathematical model embodying the mechanisms of erosion on behaviour, has been developed to predict erosion rates of coal-fired boiler components at different temperatures. Various grades of steels used in fabrication of boiler components and published data pertaining to boiler fly ash have been used for the modelling. The model incorporates high temperature tensile properties of the target metal surface at room and elevated temperatures and has been implemented in an user-interactive in-house computer code (EROSIM–1), to predict the erosion rates of various grades of steel. Predictions have been found to be in good agreement with the published data. The model is calibrated with plant and experimental data generated from a high temperature air-jet erosion-testing facility. It is hoped that the calibrated model will be useful for erosion analysis of boiler components.

Keywords. Mathematical model; erosion rate; boiler components; fly ash impingement; tensile properties; steel grades.

1. Introduction

In coal-fired power stations, about 20% of the ash produced in the boilers is deposited on the boiler walls, economisers, air-heaters and super-heater tubes. This deposited ash is subsequently discharged as slag and clinker during the soot-blowing process. The rest of the ash is entrained in the stream of flue gas leaving the boiler. These ash particles collide with the boiler steel components and cause extensive surface erosion. In advanced stages of erosion, the components get perforated, and may fail once they lose their structural integrity. Such erosion, together with the processes of blocking, fouling and corrosion, shortens the service-life of boiler components. Once this happens, the power station unit has to be shut down in order to replace the damaged components. The resulting penalty is not only the cost of replacing the components but also the cost of stoppage of power production. It is desirable, therefore, to be

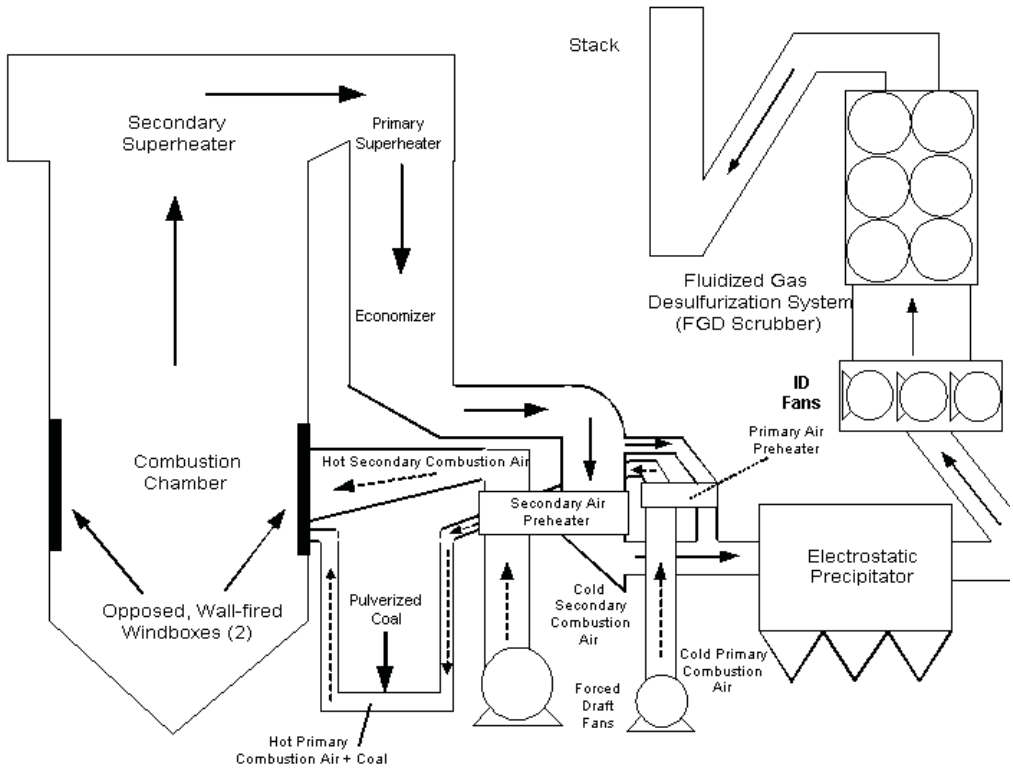

Figure 1. Coal-fired boiler assembly.

able to predict the rate of erosion of the coal-fired boiler components in order to plan systematically for the maintenance or replacement of these components and avoid forced outages. Figure 1 is a schematic of a coal-fired boiler assembly.

Various investigators have addressed the problem of solid particle erosion but the work has remained confined to room temperature investigations. Many parameters are now known to influence erosion behaviour. The magnitude and direction of an ash particle's impact velocity relative to the target metal surface constitute essential data needed for evaluating erosion of the surface due to particle impact. Magnitude and direction of a particle's rebounding velocity depend upon the conditions at impact and the specific particle–surface material combination. Restitution behaviour is a measure of the momentum lost by the particle at impact as such and it corresponds to the work done on the target surface, which, in turn, is a measure of the extent of erosion suffered by the material of the target surface. The velocity coefficients of restitution depend upon the hardness of the target material, the density of the particle and the impact velocity. Grant & Tabakoff (1975) developed empirical correlation of the velocity restitution coefficients for sand particles impacting 410 stainless steel. They used correlation in simulating the particle rebounding conditions of solid particles ingested into rotating machinery. Meng & Ludema (1995) have reviewed some of the erosion models that have been developed since Finnie (1960) proposed the first analytical erosion model. These models include a variety of parameters that influence the amount of material eroded from a target surface and the mechanism of erosion. Finnie (1960)

calculated the erosion of surfaces by solid particles by using the following derived equations

$$\varepsilon_{\mathrm{vp}} = (mV^2/P\psi k)(\sin(2\alpha) - (6/k)\sin^2\alpha), \text{ for } \tan\alpha \leq k/6, \tag{1}$$

$$\varepsilon_{\mathrm{vp}} = (mV^2/P\psi k)(k\cos^2\alpha/6) \text{ for } \tan\alpha \geq k/6, \tag{2}$$

where $\varepsilon_{\mathrm{vp}}$ is the volume of material removed by a single abrasive grain of particle, m is mass of single particle, V is velocity of particle, P is constant of plastic flow stress, ψ is the ratio of depth of contact to the depth of cut, k is thermal conductivity of the target and α is the impact angle. Subsequently, Bitter (1963) calculated the total erosion rate which is the sum of erosion due to cutting and deformation mechanisms, without including the effect of temperature, by the following derived equations.

$$\varepsilon_{\mathrm{vT}} = \varepsilon_{\mathrm{vD}} + \varepsilon_{\mathrm{vC}}, \tag{3}$$

$$\varepsilon_{\mathrm{vD}} = \tfrac{1}{2}(M(V\sin\alpha - K)^2/\delta), \tag{4}$$

$$\varepsilon_{\mathrm{vC1}} = \frac{2MV(sV\sin\alpha - K)^2}{(V\sin\alpha)^{1/2}}\left(V\cos\alpha - \frac{C(V\sin\alpha - K)^2}{(V\sin\alpha)^{1/2}}\chi\right) \text{ for } \alpha \geq \alpha_{p0}, \tag{5}$$

$$\varepsilon_{\mathrm{vC2}} = \frac{\frac{1}{2}M[V^2\cos^2\alpha - K_1(V\sin\alpha - K)^{3/2}]}{\chi}, \text{ for } \alpha \leq \alpha_{p0}, \tag{6}$$

where $\varepsilon_{\mathrm{vT}}$ is total volume erosion rate, $\varepsilon_{\mathrm{vD}}$ is volume of material removed by deformation mechanism, $\varepsilon_{\mathrm{vC}}$ is the volume of material removed by cutting mechanisms, M is total mass of impinging particle, K is velocity component normal to surface below which no erosion takes place in certain hard materials, K_1 is proportionality constant and C is constant.

Experimental and computational investigations carried out by Jun & Tabakoff (1994) and Fan *et al* (1990) have contributed to understanding the mechanisms of erosion, but the detailed processes leading to material removal are still poorly understood. This means that with a few exceptions, good models for predicting the behaviour of materials during erosion are still not readily available. Temperature is another important influencing factor in the rate of erosion. High temperature erosion behaviour is very complex owing to the variations in materials properties, degree of oxidation etc. Tilly (1969) reported results of tests on various materials up to 600°C and observed varying tendencies. Recently, the development of coal conversion and utilisation technology has accelerated the need for greater elucidation of particle-erosion behaviour, particularly at elevated temperatures. It has been observed that erosion rates of steels impacted at low angles increase as the temperature of the steel increases. Also, it is observed that rates of erosion vary depending on the type and the composition of the steel.

Hutchings & Winter (1974) concluded that the mechanism of material removal was one of shearing of the top layers of the target surface in the direction of motion of the projectiles. They carried out experimental investigations to determine the effect of erosion owing to particle orientation during oblique impact of angular particles on lead and mild steel targets. They noted that for particle incidence angles close to 90°, erosion occurred by plastic deformation of the target surface. Levy (1986) observed that the models that had been developed based on assuming micromachining of the target metal surface by the tips of eroding solid particles were faulted by not being able to predict several important aspects of measured erosion loss. He carried out experimental investigations on eroded metal surfaces using scanning electron

microscopy at high magnifications, and observed that the loss of material from an eroded metal surface occurred by a combined extrusion–forging mechanism.

Gee *et al* (2003) used a stepwise testing method for determining the mechanism of gas-borne particulate erosion. Stepwise testing is an approach that has recently been developed as a way of providing information on the build-up of damage in erosion.

The ever-increasing capability of computers has led to the development of several numerical models for gas-particle flows. Tu *et al* (1997) carried out multidimensional computational fluid dynamics (CFD) simulations of flue gas with fly ash to predict erosion of the economisers in coal-fired boilers. Lee *et al* (1999) used the Lagrangian approach while carrying out CFD simulations to predict erosion of boiler tubes by fly ash. Deng *et al* (2004), for the first time, made experimental measurements of particle rotation. This was only possible due to recent availability of advanced measurement technology. Erosion studies have been carried out in the centrifugal accelerator type erosion tester, in which the orientation of the target is varied in order to control the spin direction.

2. Mathematical erosion model

Erosion is a process in which material is removed from the surface layers of an object impacted by a stream of abrasive particles. Erosion is localised in a small volume of the target material that is eventually removed. The magnitude of the wear is quantified by the volume or mass of the material that is removed by the action of the impacting particles. It is perceived that there are three important phenomena by which metal can be removed at elevated temperatures as below.

(1) Removal of material due to cutting wear.
(2) Removal of material due to repeated plastic deformation.
(3) Effect of temperature on the tensile properties of the material.

The first two phenomena are applicable to erosion at ambient temperature, where the effect of temperature may be ignored. The relative contribution of the first two phenomena is difficult to predict due to the many process and material parameters that are involved. The effect of temperature on the erosion behaviour of boiler components is of practical importance and an attempt has been made to functionally correlate the tensile properties of these materials at elevated temperatures, which has been incorporated in the model. In the present model, the following process and materials parameters are considered for predicting erosion rate in the boiler components.

(1) Ash particle velocity, (2) ash particle impingement angle, (3) mass fraction of silica contained in the ash sample, (4) average density of ash particles, (5) density of the steel component, (6) yield stress of the steel component, and (7) temperature of the steel component.

Six steel compositions (carbon steel, 1·25 Cr–1Mo–V steel, 2·25Cr–1Mo steel, 12Cr–1Mo–V steel, 304 steel and alloy 800 steel), which are often used for high temperature boiler components, have been considered in the present modelling study. The detailed compositions of these steels (target material) are given in table 1 and the composition of typical boiler fly ash particles is listed in table 2.

2.1 *Cutting wear*

An ash particle that strikes the surface at an acute angle and at velocity greater than the critical velocity needed for the penetration of the material's surface, removes some material

Table 1. Chemical composition of various grades of steel.

	Amount (wt%) of the following metals						
Steel	C	Si	Mn	Ni	Cr	Mo	V
Carbon steel	0·22	0·28	0·65				
1·25Cr–1Mo–V	0·13	0·25	0·55		1·20	0·95	0·30
2·25Cr–1Mo	0·10	0·34	0·44		2·20	0·98	
12Cr–1Mo–V	0·19	0·33	0·59		11·40	0·87	0·28
304	0·08	0·62	1·68	10·25	18·50		
Alloy 800	0·07	0·51	1·13	32·85	20·85		

in a process similar to the cutting action of a machine tool. At the impact point, the particle loses a fraction of its kinetic energy to the target material in the form of heat and energy for deformation of the surface. Very high levels of shear strain may be induced in the material at this point. When the shear strain exceeds the elastic strain limit of the target material, the particle penetrates the surface of the material and ploughs along the surface, removing material.

During the wear process, it is assumed that the stresses acting at the contact point are constant. The ash particle penetrating the surface of the material has to overcome the material's resistance to deformation. The equation of motion for the depth of penetration, h, of a particle of mass m_p and diameter d_p, as it penetrates through the surface of a material, developed by Kragelsky *et al* (1982), has been applied in the present formulation in the form of the following differential equation,

$$m_p(\mathrm{d}^2h/\mathrm{d}t^2) = -\pi(d_p/2)hc\sigma_y, \tag{7}$$

where t is the time, σ_y the yield stress of the target material, and C a particle shape factor equal to 3 for a sphere. The negative sign in (7) accounts for the fact that the material resists the

Table 2. Chemical (elemental) composition of a typical boiler fly ash sample.

Element	Chief compound in ash	% Composition
Silicon	Silica (SiO_2)	55·20
Aluminium	Aluminium oxide (Al_2O_3)	30·80
Iron	Iron oxide (Fe_2O_3)	3·67
Titanium	Titanium oxide (TiO_2)	1·61
Phosphorus	Phosphorus pentoxide (P_2O_5)	0·35
Calcium	Calcium oxide (CaO)	5·01
Magnesium	Magnesium oxide (MgO)	1·40
Sodium	Sodium oxide (Na_2O)	0·20
Potassium	Potassium oxide (K_2O)	0·73
Sulphur	Sulphur (S)	0·20
Manganese	Manganese oxide (MnO)	0·03
Total	$SiO_2 + Al_2O_3 + Fe_2O_3$	89·67

penetrating action of the impacting particle. The mass, m_p, for a spherical particle is derived from the following simple relationship,

$$m_p = (1/6)\rho_p \pi d_p^3 \tag{8}$$

Substituting for the mass of the spherical particle, (7) can then be rewritten as

$$\mathrm{d}^2h/\mathrm{d}t^2 = -9\sigma_y h/(\rho_p d_p^2). \tag{9}$$

When a particle strikes a surface with a velocity V and at an angle of incidence β, the initial rate at which the particle penetrates into the material is equal to the normal component of the impact velocity. Equation (9) is integrated using the initial condition that at $t = 0$, $(\mathrm{d}h/\mathrm{d}t) = V \sin\beta$, and the following equation is obtained:

$$\mathrm{d}h/\mathrm{d}t = \pm[V^2 \sin^2\beta - (9\sigma_y h^2/\rho_p d_p^2)]^{1/2}. \tag{10}$$

The physical significance of the plus sign in (10) corresponds to an increase in the depth of penetration and the minus sign corresponds to a decrease in the depth of penetration. The maximum depth of penetration, $h_{\max}$, occurs when $(\mathrm{d}h/\mathrm{d}t) = 0$, and is given by the equation:

$$h_{\max}^3 = (\mathrm{d}_p^3/3^3)V^3 \sin^3\beta(\rho_p/\rho_y)^{3/2}. \tag{11}$$

Since the volume of material that is cut away from the target surface by the impacting particle is proportional to $h_{\max}^3$, the mass of material removed by a single particle is also be proportional to the value of $h_{\max}^3$. The mass of material eroded by cutting mechanism 'm_c' by a single impacting particle, thus, may be given by the following equation:

$$m_c = K_c \rho_m h_{\max}^3 = K_c \rho_m \rho_p^{3/2} d_p^3 V^3 \sin^3\beta/(3^3\sigma_y^{3/2}) \tag{12}$$

Here K_c is a constant and ρ_m the density of target material. The erosion rate due to cutting wear, defined as the ratio of the mass of the material eroded from the target surface to mass of the impacting particle, is

$$\varepsilon_c = \frac{m_c}{m_p} = \frac{K_c \rho_m \rho_p^{3/2} d_p^3 V^3 \sin^3\beta}{3^3\sigma_y^{3/2}(\pi\rho_p(d_p^3/6))} = \frac{K_1 \rho_m \rho_p^{1/2} V^3 \sin^3\beta}{\sigma_y^{3/2}}, \tag{13}$$

where K_1 is a constant.

2.2 *Plastic deformation wear*

During particle impact, loss of material because of particle erosion may occur by a combined extrusion–forging mechanism. Platelets are initially extruded from shallow craters made by the impacting particle. Once formed, the platelets are forged into a strained condition, in which they are vulnerable to being knocked off the surface in one or several pieces. Owing to the high strain rates, adiabatic shear heating occurs in the surface region immediate to the impact site. Beneath the immediate surface region, a work hardened zone forms, as the kinetic energy of the impacting particles is enough to result in a considerably greater force being imparted to the metal than is required to generate platelets at the surface. When the surface is completely converted to platelets and craters and the work-hardened zone reaches its stable hardness and thickness, steady state erosion begins. The reason why the steady state erosion rate is the

highest is because the subsurface cold-worked zone acts as an anvil, thereby increasing the efficiency of the impacting particles to extrude-forge platelets in the now highly strained and most deformable surface region. This cross-section of material moves down through the metal as erosion loss occurs. In the platelet mechanism of erosion, there is a localised sequential extrusion and forging of metal in a ductile manner, leading to removal of the micro segments thus formed.

During plastic deformation, the normal component of the particle's kinetic energy is used to extrude-forge the material. The normal component of the kinetic energy of the particle is given by

$$E_1 = \tfrac{1}{2}(\pi d_p^3/6)\rho_p V^2 \sin^2\beta = (\pi/12)\rho_p d_p^3 V^2 \sin^2\beta, \tag{14}$$

where d_p and ρ_p are the particle diameter and density respectively, and V and β the particle incident velocity and angle respectively.

The work done by the normal force N of the indenting particle, in a direction h normal to the surface from the time of surface contact until penetration stops at a depth $h_{\max}$ is given by

$$E_2 = \int_0^{h_{\max}} N \mathrm{d}h. \tag{15}$$

Sheldon & Kanhere (1972) formulated the following equation relating the force N and the diameter δ of the crater formed in the indented surface,

$$N = a\delta^n, \tag{16}$$

where constants, n and a, are given as follows

$$n = 2{\cdot}0 \quad \text{and} \quad a = \tfrac{1}{4}\pi H_V.$$

H_V is Vickers hardness number of the target surface eroded by particle impingement. Substituting (16) into (15) yields

$$E_2 = \frac{\pi H_V}{4} \int_0^{h_{\max}} \delta^2 \mathrm{d}h. \tag{17}$$

The depth of penetration, h, is related to the instantaneous crater diameter δ and the particle diameter d_p as

$$h = \tfrac{1}{2}(d_p - (d_p^2 - \delta^2)^{\frac{1}{2}}). \tag{18}$$

Equation (18) is used to express the particle's depth of penetration in terms of the instantaneous crater diameter. Equation (17) may be integrated with respect to the instantaneous crater diameter. Equating the work done during indention to the normal component of kinetic energy given in (14), the following equation is obtained,

$$\frac{\pi}{12} d_p^3 \rho_p V^2 \sin^2\beta = \frac{\pi H_V}{8} \int_0^{h_{\max}} \frac{\delta^2 d\delta}{(d_p^2 - \delta^2)^{1/2}}. \tag{19}$$

The integral in (19), is evaluated and the maximum depth of penetration is derived as

$$h_{\max}^3 = d_p^3 V^3 \sin^3 \beta \rho_p^{3/2} / H_V^{3/2}. \tag{20}$$

Since the dimensions of the crater formed by the impacting particle are all proportional to $h_{\max}^3$, and since the amount of material removed is nearly of full crater size, the mass of material removed by a single particle is proportional to the value of $h_{\max}^3$ derived in (20). The mass 'm_d' of material removed by plastic deformation by a single particle is given by the following equation,

$$m_d = K_p \rho_m h_{\max}^3 = K_p \rho_m \rho_p^{1/2} (d_p^3 V^3 \sin^3 \beta / H_V^{3/2}), \tag{21}$$

where K_p is a constant and ρ_m is the density of the target material. The erosion rate, ε_p, due to plastic deformation is given by the following,

$$\varepsilon_p = \frac{m_d}{m_p} = \frac{K_p \rho_m \rho_p^{1/2} d_p^3 V^3 \sin^3 \beta}{H_V^{3/2} (\rho_p \pi d_p^3 / 6)} = \frac{K_2 \rho_m \rho_p^{1/2} V^3 \sin^3 \beta}{H_V^{3/2}}, \tag{22}$$

where K_2 is a constant.

2.3 *Overall erosion rate and effect of temperature*

The erosion of the boiler components by fly ash consists of the wear due to the cutting mechanism plus the wear due to plastic deformation. However, it is difficult to predict accurately the separate contributions by each of the two mechanisms to the overall material loss. Equation (22), which was derived for plastic deformation wear, is similar to (13) for cutting wear. The yield stress of a metal can be related to the metal's hardness. Tabor (1951) has proposed the following empirical relationship between the yield stress and Vickers hardness number,

$$H_V = 2{\cdot}7 \sigma_y. \tag{23}$$

The overall erosion rate, combining the cutting and plastic deformation wear mechanisms, is then given as

$$\varepsilon = K_3 \rho_m \rho_p^{1/2} V^3 \sin^3 \beta / \sigma_y^{3/2}, \tag{24}$$

where K_3 is a constant which is documented in the literature (Tabor 1951; Finnie 1960; Fan *et al* 1990; Jun & Tabakoff 1994; Meng & Ludena 1995). From the studies carried out by various investigators (Sheldon & Kanhere 1972; Sheldon *et al* 1977; Fan *et al* 1990; Jun & Tabkoff 1994), the erosion rate due to solid particle impact is found to depend upon the particle impingement angle and the characteristics of the particle-wall combination for modelling erosion of ductile metal surfaces by fly ash. The constant K_3 in (24) may be replaced by the particle erosion index giving the expression for the overall erosion rate,

$$\varepsilon = K_e I_e(x) \rho_m \rho_p^{1/2} V^3 \sin^3 \beta / \sigma_y^{3/2}, \tag{25}$$

where K_e is a constant, x the mass fraction of silica contained in the ash sample, and I_e the erosion index of the ash, which relates the variation of the erosion rate to the silica content.

The temperature effect can be introduced on the basis of the observation that the erosion rate at acute impingement angle increases significantly with temperature, suggesting that steel

tends to show behaviour more typical of a ductile material at elevated temperatures. The yield stress (kgf/mm^2) and temperature (K) functionality has been derived through a polynomial approximation for various grades of steel on the basis of the available tensile property data (Lee *et al* 1999). The following expressions have been generated.

• Carbon steel

$$\sigma_y = 2 \times 10^{-5} \times T^2 - 0{\cdot}0353 \times T + 30{\cdot}871. \tag{26}$$

• Cr–1Mo–V steel

$$\sigma_y = -2 \times 10^{-5} \times T^2 - 0{\cdot}0278 \times T + 48{\cdot}703. \tag{27}$$

• 2·25Cr–1Mo steel

$$\sigma_y = -5 \times 10^{-8} \times T^3 + 10^{-5} \times T^2 - 0{\cdot}0133 \times T + 33{\cdot}324. \tag{28}$$

• 12Cr–1Mo–V steel

$$\sigma_y = -5 \times 10^{-7} \times T^3 + 0{\cdot}0005 \times T^2 - 0{\cdot}1379 \times T + 59{\cdot}169. \tag{29}$$

• 304 steel

$$\sigma_y = -2 \times 10^{-8} \times T^3 + 6 \times 10^{-5} \times T^2 - 0{\cdot}0485 \times T + 28{\cdot}179. \tag{30}$$

• Alloy (Incoloy) 800

$$\sigma_y = -5 \times 10^{-8} \times T^3 + 7 \times 10^{-5} \times T^2 - 0{\cdot}036 \times T + 20{\cdot}858. \tag{31}$$

3. Numerical implementation

The model has been implemented in a user-interactive computer code (EROSIM-1) which embodies the solid particle erosion mechanism due to cutting wear and repeated plastic deformation. The overall erosion is estimated from the contributions of both the mechanisms of wear. The code predicts the erosion rate in terms of the weight (mg) of the target material removed per weight (kg) of the impacting fly ash particle as a function of impact velocity, impact angle, density and silica content of the ash particle, and density and yield stress of the target material. Erosion behaviour at elevated temperatures has been incorporated through the derived functionality of the tensile property (yield stress) with temperature using (26)–(31) with appropriate modification of yield strength.

4. Results and discussion

Some typical results of model predictions are presented in figures 2 and 3 showing the variation of erosion rate with velocity, at impingement angle of 30° and room temperature for carbon steel and 1·25Cr–1Mo–V steel respectively. It may be observed that there is an increase in erosion rate with increasing impacting particle velocity in both cases. In figure 3, the predicted result is verified with the published experimental data at room temperature which are superimposed on the theoretical predictions and found to be in good agreement

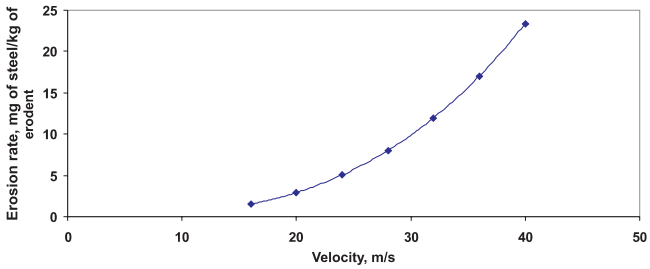

Figure 2. Variation of erosion rate with impingement velocity (carbon steel), impingement angle = 30°, room temperature.

(Sheldon & Kanhere 1972; Winter & Hutchings, 1974; Sheldon *et al* 1977; Shida & Fujikana 1985). Figures 4, 5 and 6 show the variation of erosion rate with temperature for carbon steel, 1·25Cr–1Mo–V steel and alloy 800 steel respectively. A tendency for erosion rate to increase with temperature has been observed in all steels. Thus, it may be concluded that the erosion rate of steels impacted at low angles definitely increases as the temperature is increased. Also, the rates of erosion are significantly different depending on the type of the steel. Figures 7 and 8 show the erosion rate as a function of particle impact angle for carbon steel and 1·25Cr–1Mo–V steel respectively, at room temperature (303 K) and at elevated temperatures of 573 K and 873 K. It is observed that at all temperature levels, for low impingement angle, the erosion rate increases with increase in the impingement angle until a maximum value is reached at an angle between 25° and 30°. Thereafter the erosion rate falls off rapidly. Comparison of experimental data with the theoretical predictions is shown in figure 8. The order of magnitude of erosion rate and the erosion behaviour as a function of impingement angle for a typical ductile material are found to be fully consistent with the reported experimental data (Sheldon & Kanhere 1972; Sheldon *et al* 1977; Shida & Fujikana 1985). Figures 9 and 10 show the erosion rate as a function of particle impact velocity for carbon steel and 1·25Cr–1Mo–V steel respectively, at three temperatures: 303, 573 and 873 K. At elevated temperatures also, the erosion rate increases monotonically with increase in particle impingement velocity. The model-based code (EROSIM-1) has been validated as a predictive tool for solid particle erosion analysis of coal-fired boiler components.

5. Conclusion

A model to predict the erosion rate for fly ash particle impingement on boiler component surfaces has been developed and the variation of erosion rate with various parameters investigated and found to be in good agreement with the published experimental data. It is seen that the erosion rates on steel surfaces subjected to a stream of fly ash particles vary with the particle impingement angle. For low values of impingement angle, erosion rate increases with increase in impingement angle, with the maximum erosion rate occurring at an impingement angle of about 30°. Thereafter, erosion rate decreases with further increase in impingement angle. It is also noted that erosion rates at low impingement angles increase significantly with increasing temperature, but at high impingement angles the effect of temperature is insignificant. All the steel grades investigated in this study show increase in erosion rates with temperature. Variation of erosion rate shows monotonic rise with ash particle impact velocity. The code has been validated with the published information. Ash particle impact angle, which is one of the important parameters influencing erosion rate, requires further study. The influence of the shape and rotation angle of ash particles on erosion rates also needs further investigation using appropriate mathematical models

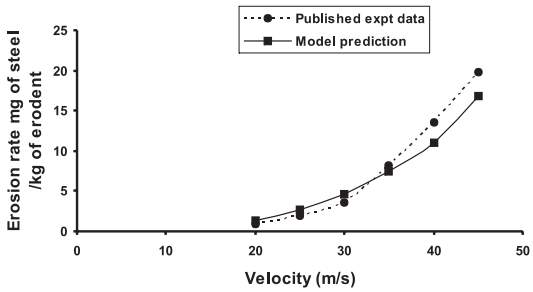

Figure 3. Variation of erosion rate with impingement velocity (1·25 Cr-1Mo-V steel), impingement angle = 30°, room temperature (303 K).

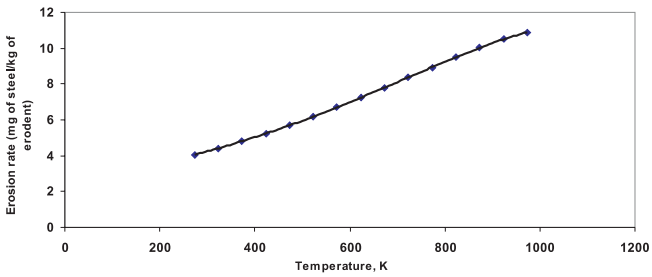

Figure 4. Variation of erosion rate with temperature of target material (carbon steel), impingement angle = 30°, impingement velocity = 19·41 m/s.

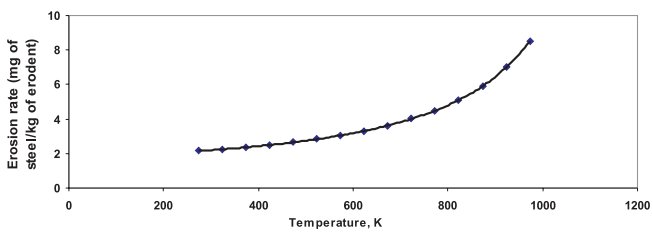

Figure 5. Variation of erosion rate with temperature of target material (1·25Cr-1Mo-V steel), impingement angle = 30°, impingement velocity = 19·41 m/s.

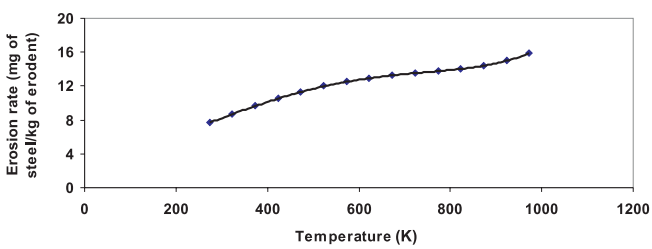

Figure 6. Variation of erosion rate with temperature of target material (alloy 800 steel), impingement angle = 30°, impingement velocity = 19·41 m/s.

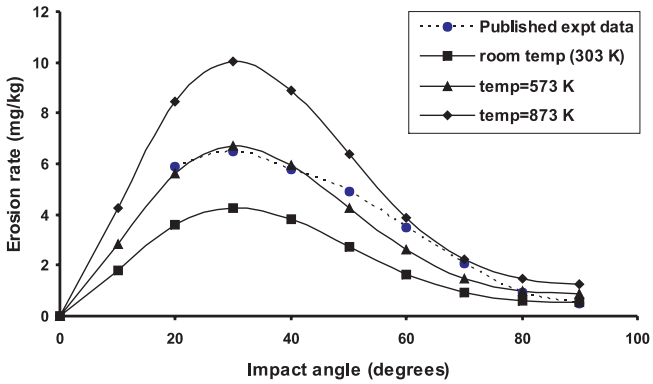

Figure 7. Variation of erosion rate with impingement angle at room temperature and elevated temperatures at 573 K and 873 K (carbon steel).

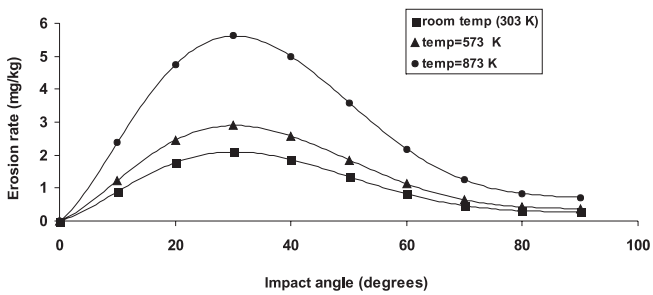

Figure 8. Variation of erosion rate with impingement angle at room temperature and elevated temperatures at 573 K and 873 K (1·25Cr-1Mo-V steel).

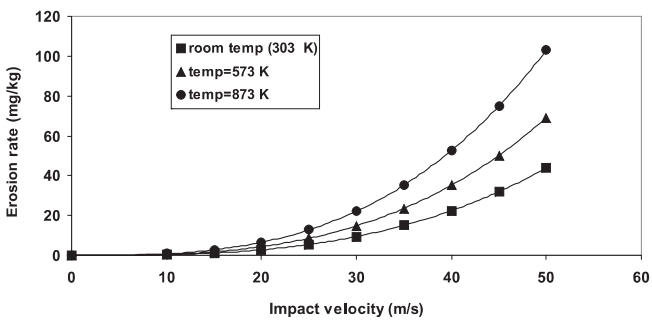

Figure 9. Variation of erosion rate with impact velocity at room temperature and elevated temperatures at 573 K and 873 K (carbon steel).

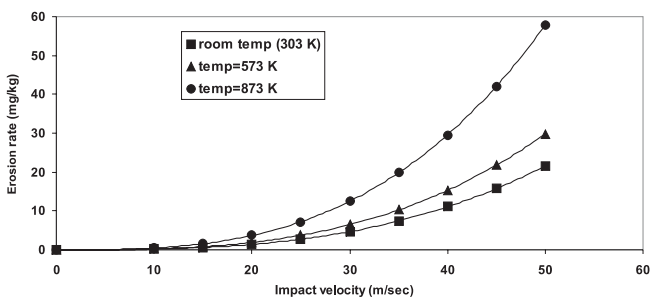

Figure 10. Variation of erosion rate with impact velocity at room temperature, and elevated temperatures at 573 K and 873 K (1·25Cr-1Mo-V steel).

References

Bitter J G A 1963a A study of erosion phenomenon, Part 1. *Wear* 6: 5–21

Bitter J G A 1963b A study of erosion phenomenon, Part 2. *Wear* 6: 169–191

Deng T, Bingley M S, Bradley M S A 2004 The influence of particle rotation on the solid particle erosion rate of metals. *Wear* 256: 1037–1049

Fan J Cen D, Zhou K, Jin J 1990 Numerical prediction of tube row erosion by coal ash impaction. *Chem. Eng. Commun.* 95 :75–88

Finnie I 1960 Erosion of surfaces by solid particles. *Wear* 142: 87–103

Gee M G, Gee R H, McNaught I 2003, Stepwise erosion as a method for determining the mechanisms of wear in gas borne particulate erosion. *Wear* 255: 44–55

Grant G, Tabakoff W 1975 Erosion prediction in turbomachinery resulting from environmental solid particles. *J. Aircraft* 12: 471–478

Hutchings I M, Winter R E 1974 Particle erosion of ductile metals: a mechanism of material removal. *Wear* 27: 121–128

Jun Y D, Tabakoff W 1994 Numerical simulation of a dilute particulate flow (laminar) over tube banks. *Trans. ASME: J. Fluid Eng.* 116: 770–777

Kragelsky I V, Dobychin M N Komalov V S 1982 *Friction and wear calculation methods* (New York: Pergamon)

Lee B E, Fletcher C A J, Behnia M 1999 Computational prediction of tube erosion in coal-fired power utility boilers. *J. Eng. Gas Turbines Power* 121: 746–750

Levy A V 1986 The platelet mechanism of erosion of ductile metals. *Wear* 180: 1–21

Meng H C, Ludema K C 1995 Wear models and predictive equations: Their form and content. *Wear* 181-183: 443–457

Sheldon G I, Kanhere A 1972 An investigation of impingement erosion using single particles. *Wear* 21: 195–209

Sheldon G L, Maji J, Crowe C T 1977 Erosion of a tube by gas-particle flow. *Trans. ASME: J. Eng. Mater. Technol.* 99 : 138–142

Shida Y Fujikawa H 1985 Particle erosion behaviour of boiler tube materials at elevated temperature. *Wear* 103: 281–296

Tabor D 1951 *The hardness of metals* (Oxford: University Press)

Tilly G P 1969 Erosion caused by airborne particles. *Wear* 14: 63–79

Tu J Y, Fletcher C A J, Behnia M, Reizes J A, Owens D, Jones P 1997 Prediction of flow and erosion in power utility boilers and comparison with measurement. *J. Eng. Gas Turbines Power* 119: 709–716

Winter R E Hutchings I M 1974 Solid particle erosion studies using single angular particles. *Wear* 29: 181–194